ChemPubSoc Europe

DOI: 10.1002/chem.201406199

CHEMISTRY
A European Journal
Full Paper

Mesoporous Materials

Hierarchically Designed Three-Dimensional Macro/Mesoporous Carbon Frameworks for Advanced Electrochemical Capacitance Storage

Yanbing Yang,[a, b] Peixu Li,[c, d] Shiting Wu,[b] Xinyang Li,[a] Enzheng Shi,[b] Qicang Shen,[d] Dehai Wu,[d] Wenjing Xu,[b] Anyuan Cao,*[b] and Quan Yuan*[a]

Abstract: Mesoporous carbon (m-C) has potential applications as porous electrodes for electrochemical energy storage, but its applications have been severely limited by the inherent fragility and low electrical conductivity. A rational strategy is presented to construct m-C into hierarchical porous structures with high flexibility by using a carbon nanotube (CNT) sponge as a three-dimensional template, and grafting Pt nanoparticles at the m-C surface. This method involves several controllable steps including solution deposition of a mesoporous silica (m-SiO_2) layer onto CNTs, chemical vapor deposition of acetylene, and etching of m-SiO_2, resulting in a CNT@m-C core–shell or a CNT@m-C@Pt core–shell hybrid structure after Pt adsorption. The underlying CNT network provides a robust yet flexible support and a high electrical conductivity, whereas the m-C provides large surface area, and the Pt nanoparticles improves interfacial electron and ion diffusion. Consequently, specific capacitances of 203 and 311 $F g^{-1}$ have been achieved in these CNT@m-C and CNT@m-C@Pt sponges as supercapacitor electrodes, respectively, which can retain 96% of original capacitance under large degree compression.

Introduction

A fast-growing need for portable electronic devices has promoted the development of high-power energy-storage systems. Supercapacitors combine the benefits of high rate capacity and long cyclic life, and have stimulated extensive research interest. Design and fabrication of efficient electrodes and hybrid structures is critical for the development of supercapacitors. Porous materials with a high surface area and suitable pore size could potentially improve capacitance by facilitating ion transport/diffusion and maximizing the surface area accessible to electrolyte ions.[1] Porous carbon-based materials with controlled pore sizes, structures, and chemical stability in various solutions have been extensively investigated as an ideal electrical double-layer capacitor (EDLC).[2] Among those, mesoporous carbon (m-C) has been synthesized in the form of powders, fibers, composites, monoliths, tubes, and explored as supercapacitor electrodes.[3] However, there are two challenges facing the m-C material in energy applications, namely 1) the intrinsic poor electrical conductivity arises from a large number of defective sites such as broken and dangling bonds, unpaired electrons and oxidized carbon sites in its amorphous structure; and 2) its inherent fragility limits its application as flexible electrodes.

Carbon nanotubes (CNTs) are one-dimensional tubular structures with outstanding electrical conductivity and mechanical flexibility. The electronic transport along the CNT axis is very efficient without scattering over a long distance. Introducing CNTs into a m-C matrix is a promising way to fabricate hybrid systems with enhanced electrical conductivity and also to achieve mechanical flexibility. Random combination of CNTs and m-C to fabricate nanocomposites cannot improve electrical conductivity substantially because CNTs are not contacted very well in the mixture and there is a poor interface between CNTs and m-C.[4,5] Furthermore, the lack of interconnected macropores in the composite strongly limits mass transportation and charge accumulation. It remains a big challenge to fabricate hybrid CNT and m-C systems with high controlled porous structure, high flexibility, and conductivity.

[a] Y. Yang, X. Li, Prof. Q. Yuan
Key Laboratory of Analytical Chemistry for Biology and Medicine (Ministry of Education)
College of Chemistry and Molecular Sciences,
Wuhan University, Wuhan 430072 (P.R. China)
E-mail: yuanquan@whu.edu.cn

[b] Y. Yang, S. Wu, E. Shi, W. Xu, Prof. A. Cao
Department of Materials Science and Engineering
College of Engineering, Peking University
Beijing 100871 (P.R. China)
E-mail: anyuan@pku.edu.cn

[c] Dr. P. Li
Aeronautical Manufacturing Technology Institute
Shanghai Aircraft Manufacturing Co., Ltd
Shanghai 200436 (P.R. China)

[d] Dr. P. Li, Q. Shen, Prof. D. Wu
Department of Mechanical Engineering
Tsinghua University, Beijing 100084 (P.R. China)

Supporting information for this article (including the Experimental Details) is available on the WWW under http://dx.doi.org/10.1002/chem.201406199.

Here, we present a rational strategy to construct m-C-based hierarchical architectures by adopting a CNT sponge as a 3D template combined with Pt adsorption. The resulting CNT@m-C@Pt core–shell hybrid structure shows graphitized m-C coating with close contact to CNTs. Whereas the CNT network provides a robust yet flexible support and high electrical conductivity, the macropores among the CNT network allow fast mass transport throughout the sponge and ensure efficient electrolyte diffusion to mesopores and micropores. Furthermore, Pt nanoparticles grafted on m-C also act as diffusion channels for electrolyte ions and electrons to the electrodes.[6] We used these CNT@m-C@Pt sponges to fabricate flexible supercapacitor electrodes with specific capacitances up to 311 $F g^{-1}$ and stable performance under large degree compression. The optimized and tunable microstructure may lead to a further development of high-electrochemical energy-storage systems based on m-C materials.

Results and Discussion

We utilized a CNT sponge as a 3D porous template to deposit m-C and form two types of hierarchical structures including a CNT@m-C core–shell and a CNT@m-C@Pt core–shell hybrid sponge (after Pt adsorption), as illustrated in Scheme 1a. The CNT sponges reported by our group are composed by 3D stacked multiwalled nanotube networks with low density (close to aerogels), high electrical conductivity, and excellent mechanical flexibility.[7] First, we coated mesoporous silica (m-SiO_2) as a sacrificial layer onto the CNT network by using a sol–gel reaction as described in our earlier report.[8] Then, we adopted chemical vapor deposition (CVD) to decompose C_2H_2 into the pores of m-SiO_2 as a conformal carbon layer, and obtained a graphitized m-C layer by removing m-SiO_2. Based on the CNT@m-C network, Pt nanoparticles are grafted onto the m-C layer by solution adsorption. Scheme 1a illustrates the entire process starting from CNTs to the CNT@m-SiO_2, CNT@m-C, and finally CNT@m-C@Pt structures (see the Experimental Section for details in the Supporting Information). Scheme 1b shows the 3D porous structural model of the initial CNT sponge and the CNT@m-C@Pt core–shell hybrid sponge in bulk forms. This is an optimized hierarchical structure in which the CNT conductive network is well preserved by a uniform m-C coating.

Scanning electron microscopy (SEM) and transmission electron microscopy (TEM) characterization at each fabrication step reveal two features related to the morphology and structure of our sponges. First, the m-SiO_2 and m-C coatings are uniform throughout the sponge and the coating thickness can be well controlled. Second, the macroscopic sponge maintains its highly porous structure after coating, and the interconnected CNT network is not disturbed. This is important for preserving the original CNT contact in the sponge and maintaining a high conductivity of the hybrid structure. The original CNT sponge consists of randomly overlapped multiwalled nanotubes with diameters of about 30 nm (Figure 1a). Successful coating of m-SiO_2 and m-C can be seen from the CNT diameter change after each step, which increases to about 40 nm (after coating m-C; Figure 1b,c). At the same time, the initial black color of the CNT sponge changes to gray after coating m-SiO_2, and then changes to black after coating m-C and etching m-SiO_2 (Figure 1d). The CNT@m-C sponge maintains a similar structure compared to the original CNT sponge, particularly the 3D network and high porosity (Figure 1c).

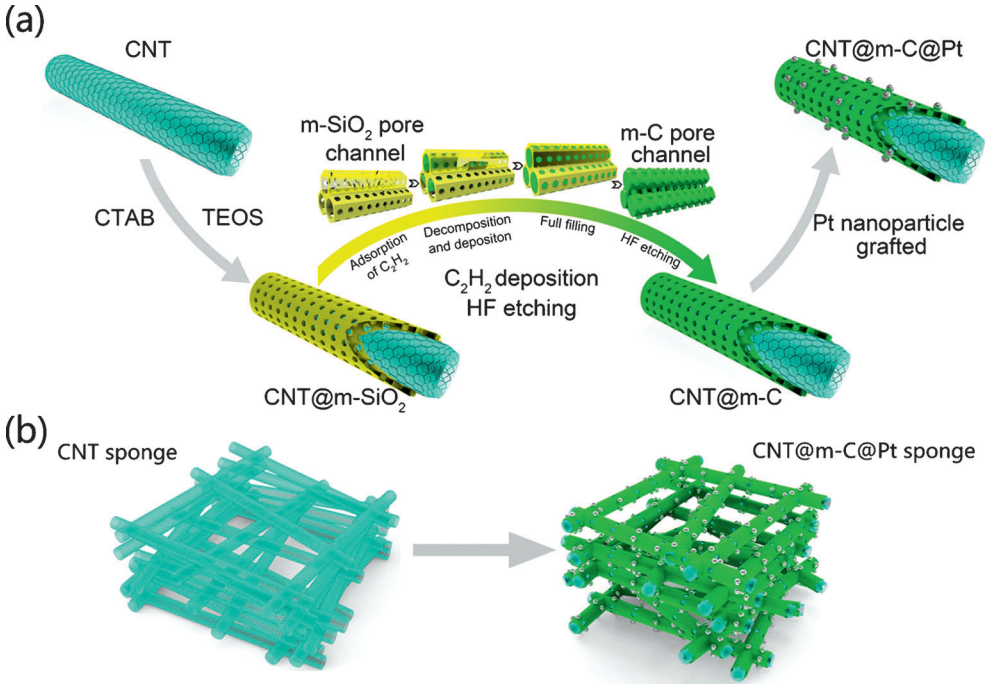

Scheme 1. Illustration of the fabrication process of CNT@m-C@Pt sponges. a) Synthetic process starting from CNTs to CNT@m-SiO_2, and then CNT@m-C, and finally CNT@m-C@Pt microstructures. b) Macroscopic models of a bulk CNT and a CNT@m-C@Pt sponge.

The TEM image of the CNT@m-SiO_2 sponge shows that the CNT surface has been coated by a uniform m-SiO_2 layer with 2 nm pores and a layer thickness of about 5 nm (Figure 2a). After C_2H_2 deposition and m-SiO_2 removal, the resulting CNT@m-C sponge shows a core–shell structure in which the inside CNT cavities can be clearly seen (Figure 2b). The m-C layer has a similar thickness (ca. 5 nm) with m-SiO_2, indicating that the m-SiO_2 acts as the hard template for m-C formation. Previously, the liquid impregnation method involved a long-term reaction cycle and subsequent carbonization process, and the etching of m-SiO_2 may result in large voids and dense carbon shells. In contrast,

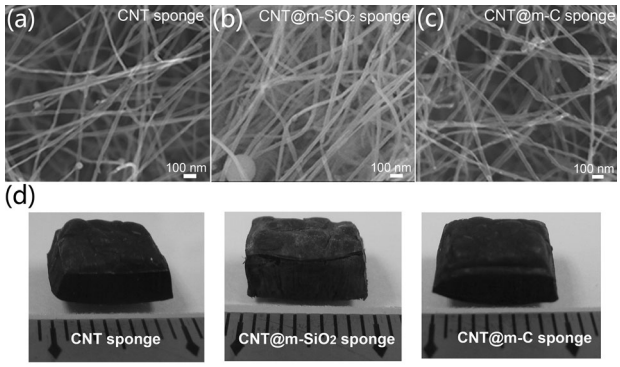

Figure 1. Structural characterization of CNT and hybrid sponges. SEM images of a) CNT, b) CNT@m-SiO_2, and c) CNT@m-C sponge, respectively. d) photos of the corresponding CNT, CNT@m-SiO_2, and CNT@m-C bulk sponges.

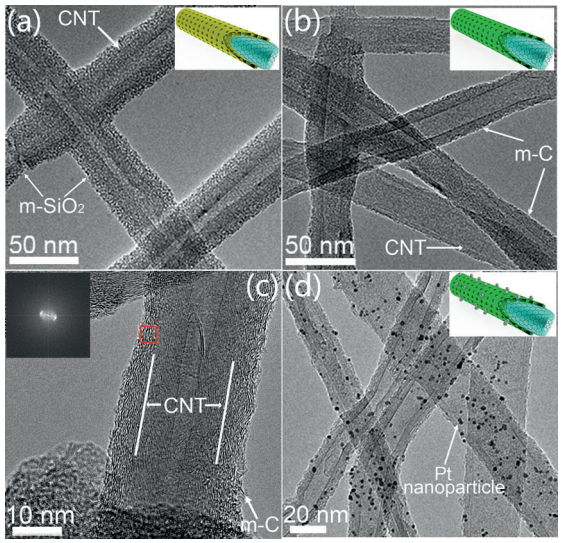

Figure 2. Structural characterization of CNT and hybrid sponges. TEM images of a) CNT@m-SiO_2, b) CNT@m-C, c) high-resolution TEM image of a CNT@m-C core–shell structure, and d) CNT@m-C@Pt structures. Insets (a, b, and d) are the structural models for the CNT@m-SiO_2, CNT@m-C, CNT@m-C@Pt nanostructures; Inset (c) is the fast Fourier transform of the selected red area of the m-C shell.

our CNT@m-C core–shell structure obtained by the CVD process retains the favorable contact between CNTs and m-C shells, suggesting the mean free path diffusion of C_2H_2 molecules into the m-SiO_2 pores prior to decomposition. The direct contact between CNTs and m-C facilitates fast interfacical electron transport. Furthermore, the graphitized m-C layer with a lamellar morphology can be observed from the high-resolution TEM image, and the interplanar spacing is 0.4 nm according to fast Fourier transform image in the selected area of the m-C layer (inset in Figure 2c). The graphitization may be derived from the coexistance of m-SiO_2 and the iron catalyst,[9–12] resulting in graphitized m-C with improved electric conductivity than that of amorphous carbon. Finally, Pt nanoparticle adsorption results in the formation of a CNT@m-C@Pt core–shell hybrid structure, in which the m-C shell acts as a substrate for hybridizing nanoparticles (Figure 2d). Due to the mesoporous morphology of m-C, Pt nanoparticles with diameters of 2 nm distribute uniformly on its surface without producing aggregations.

The structure of CNT and hybrid sponges has been fully characterized by using other techniques, including X-ray photoelectron spectroscopy (XPS), Raman, and thermogravimetric analysis (TGA). The original CNT sponge only shows a C1s peak, whereas there is a strong O1s and a Si2p peak appearing in the CNT@SiO_2 sponge (Figure 3a). The C1s peak becomes strong again in the CNT@m-C sponge, and a Pt4f peak

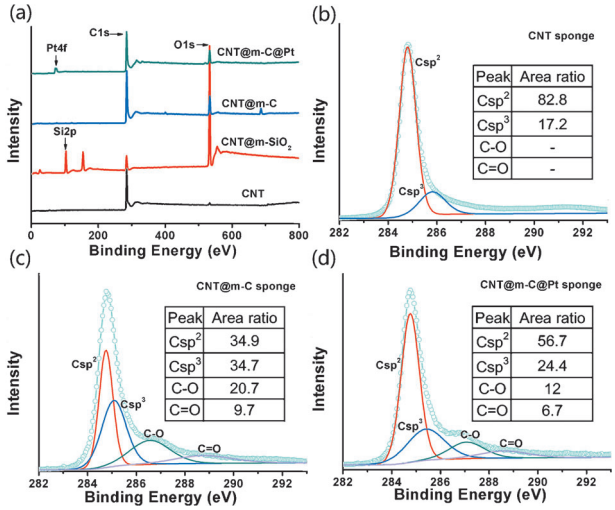

Figure 3. Spectroscopy analysis of CNT and hybrid sponges. a) XPS wide-scan spectra of the CNT, CNT@m-SiO_2, CNT@m-C, and the CNT@m-C@Pt sponge. b), c), d) High-resolution XPS spectra of the deconvoluted C1s peak: b) CNT, c) CNT@m-C, and d) CNT@m-C@Pt sponge. Insets (b, c, and d) are the corresponding area ratio of Csp^2, Csp^3, C—O, and C═O for CNT, CNT@m-C, and CNT@m-C@Pt sponges, respectively.

could be found in the final CNT@m-C@Pt sponge. The XPS results are consistent with the structural change of the sponge during each fabrication stage. From the N_2 adsorption–desorption curves, the surface area has increased from 59 (CNT sponge) to 201 $m^2 g^{-1}$ (CNT@m-C sponge) with a total pore volume of 0.3 $cm^3 g^{-1}$, due to the mesoporous coating on the CNT surface (Supporting Information, Figure S1). Pore size distribution curves also show an increased percentage of mesopores in the range of 2–50 nm after m-C coating. Raman spectra indicate an increase of the D-band in the CNT@m-C sponge (Supporting Information, Figure S1c). TGA results show a two-stage combustion process in the CNT@m-C sponge, in which the m-C layer is burned first and the CNTs combustion temperature is delayed to 630 °C compared with the CNT sponge (600 °C; Supporting Information, Figure S1d).

We have measured the electrical conductivities of CNT sponges by a four-probe method with silver paint and wire electrodes (all of the samples were compressed to similar thicknesses of about 40 μm). Whereas the original CNT sponges have conductivities of 12–15 $S cm^{-1}$, the CNT@m-C and CNT@m-C@Pt sponges are in the ranges of 26–35 and 29–36 $S cm^{-1}$, respectively. This shows that the CNT@m-C and

CNT@m-C@Pt sponges have comparable electrical conductivities, which are higher than the CNT sponges. The increase of electrical conductivity is probably due to the m-C coating throughout the CNT network, which could improve the electrical transport across the contact points between CNTs. At the same time, we did not see much influence on electrical conductivity for Pt nanoparticles dispersed and isolated on CNT@m-C. Under compression to strains of 20 and 50%, the electrical conductivities of three sponge electrodes increase slightly, possibly due to more close packing of CNTs (Supporting Information, Figure S2).

Our hierarchical macro/mesopore CNT@m-C sponges have several distinct advantages that make them ideal candidates as bulk porous supercapacitor electrodes without adding any binder. First, the well-preserved CNT skeleton provides a highly conductive 3D network throughout the sponge, which is important in achieving high electrical conductivity and efficient charge transport in porous electrodes. Second, the graphitized m-C layer uniformly coated within the sponge offers numerous mesopores and high surface area that are accessible to ions and charge accumulation. The m-C layer also serves as a substrate for anchoring Pt nanoparticles. Finally, the interconnected macropores (inter-CNT spacing) derived from the CNT network allow fast mass transport and ion diffusion, fully utilizing the internal area of the sponge. Cyclic voltammetry (CV) and galvanostatic charge–discharge (GC) characteristics were tested in a three-electrode electrochemical setup in 6 M KOH aqueous electrolyte. Compared with CNT sponges, the CNT@m-C and CNT@m-C@Pt sponges exhibit significantly enlarged rectangular CV curves at the same scan rate (100 mV s^{-1}), indicating improved supercapacitor performance (Figure 4a). The broad peaks in the corresponding CV curves are likely attributed to the pseudocapacitance, which originates from the surface oxides inevitably introduced in the preparation process. As shown in Figure 3c,d, the representative deconvoluted spectrum for CNT@m-C and CNT@m-C@Pt sponge, respectively, we can see that an increased amount of C–O (epoxy) and C=O (carbonyl) formed compared with the original CNT sponge (Figure 3b) in the fabrication process. Furthermore, the increased area percentage of C–C is derived from the defects of the m-C layer, and this defect can introduce more active sites for ion accumulation. However, in contrast to nitrogen-related pseudocapacitance, our electrode materials show stable capacitance performance even after 1000 cycles (Supporting Information, Figure S9). These three sponges also show nearly triangular GC curves measured at a high current density of 2 A g^{-1} (Figure 4b). This indicates the formation of an efficient electrochemical double layer and fast ion transport within the sponge. The specific capacitances calculated from GC curves (based on the total weight of a single electrode, sum of the CNT sponge and m-C or Pt weight) are 23, 178, and 290 F g^{-1} (at 2 A g^{-1}) for CNT, CNT@m-C, and CNT@m-C@Pt sponges, respectively. From Figure 4c,d, the voltage versus time profiles in a wide range of current densities for the CNT@m-C and CNT@m-C@Pt sponge, respectively, are shown. A quick I–V response even in the ultrahigh current density of 20 A g^{-1} indicates superior capacitance characteristics of our sponge electrodes. We also measured the specific capacitances from CV curves over a wide range of scan rates (Figure 5). The highest gravimetric capacitances are 27, 203, and 311 F g^{-1} for CNT, CNT@m-C, and CNT@m-C@Pt sponges (at 2 mV s^{-1}), respectively, which are comparable to the capacitances calculated from GC curves. The CNT@m-C@Pt sponge retains a capacitance of 243 F g^{-1} (nearly 80% retention) as the scan rate increases to 200 mV s^{-1}. The volumetric capacitance of porous electrode is a key parameter to evaluate the performance of porous electrodes, and our constructed structure show increased capacitance (at different scan rates) relative to the original CNT sponge (0.3 F cm^{-3}) by 6 (1.7 F cm^{-3}) and 9 (2.7 F cm^{-3}) folds for the CNT@m-C and CNT@m-C@Pt sponge, respectively.

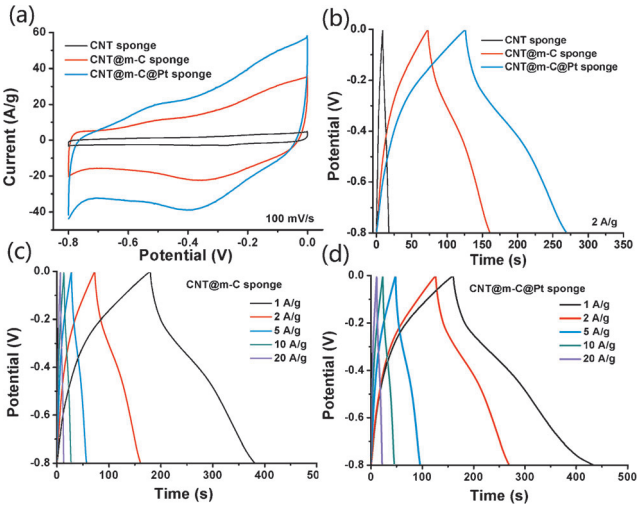

Figure 4. Supercapacitor application of the CNT and hybrid sponges. a) CV curves of the CNT, CNT@m-C, and CNT@m-C@Pt sponges at a scan rate of 100 mV s^{-1}. b) Galvanostatic charge–discharge curves of the CNT, CNT@m-C, CNT@m-C@Pt sponges at a current density of 2 A g^{-1}. c),d) GC curves of CNT@m-C and CNT@m-C@Pt sponge at different current densities.

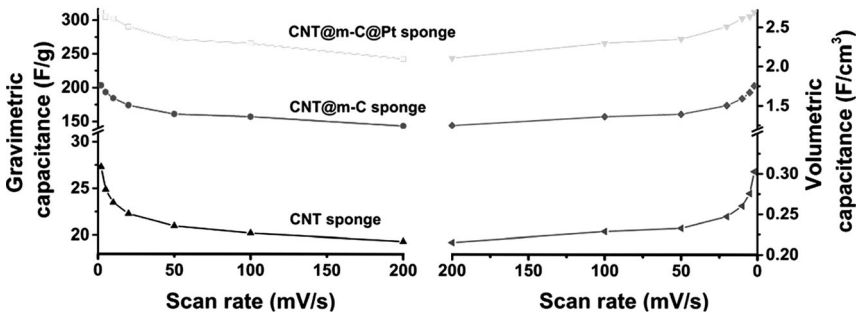

Figure 5. Calculated gravimetric and volumetric capacitances of the CNT, CNT@m-C, and CNT@m-C@Pt sponges at different scan rates.

Here, both m-C and Pt nanoparticles have a considerable effect on the supercapacitor behavior of CNT sponges. Whereas m-C mainly provides mesopores and high surface area for the electrochemical double layer capacitance, the Pt nanoparticles with excellent ionic and electronic conductivity act as an intercalator to provide diffusion channels for electrolyte ions and electrons to the electrode.[6] Uniform dispersion of isolated Pt nanoparticles does not influence the exposure and available surface area of m-C to the electrolyte. The synergistic effect of the CNT network, m-C layer, and Pt nanoparticles leads to an enhanced performance compared with that of traditional m-C-based materials. For example, a m-C electrode containing the powder form of m-C mixed with poly(tetrafluoroethylene) binder showed a specific capacitance of 143 F g^{-1} (Table 1).[14]

Table 1. Comparison of the specific capacitance between CNT@m-C@Pt sponge electrode and several reported porous carbon-based electrodes.

Material[a]	Electrolyte	Morphology	Capacitance [F g^{-1}]	Refs.
AC	30% KOH	Powder	100	[13]
N-MCS	5 M H_2SO_4	Powder	211	[3]
OMC	6 M KOH	Powder	143	[14]
Macro/micro-C aerogel	6 M KOH	Monolith	180	[15]
m-C fiber	1 M KOH	Powder	152	[3e]
CNT@m-C	6 M KOH	Powder	60	[4]
Micro/meso-C	1 M H_2SO_4	Powder	200	[16]
CNT@m-C@Pt	6 M KOH	Freestanding, flexible	311	This work

[a] AC = activated carbon, N-MCS = nitrogen-enriched mesoporous carbon sphere, OMC = ordered mesoporous carbon, macro/micro-C = macroporous/microporous carbon, m-C fiber = mesoporous carbon fiber, CNT@m-C = mesoporous carbon-coated CNT, micro/meso-C = microporous/mesoporous carbon.

In comparison, our CNT@m-C and CNT@m-C@Pt electrodes show higher specific capacitances (203 and 311 F g^{-1}, respectively) than that of the m-C electrode (Table 1). Also, our electrodes do not use binder agent or conductive additives compared with the powder form of m-C. On the other hand, Pt nanoparticles were also introduced to stainless steel current collectors or grafted onto reduced graphene oxide, leading to enhanced electrochemical performance with specific capacitances of 151 and 154 F g^{-1}, respectively.[6]

Electrochemical impedance spectroscopy (EIS) confirmed the fast ion transport and very low internal resistance of the sponge electrode (Figure 6a). The sponges display a pure capacitance behavior at frequencies of up to 176 Hz. The characteristic frequency f_0 for the CNT, CNT@m-C, and CNT@m-C@Pt sponge at phase angle of 45° is 215, 317, and 1221 Hz, respectively, whereas the corresponding time constant τ_0 (= $1/f_0$) is 4.6 and 3.1 ms for the CNT sponge and after coating m-C, respectively, and further decreases to 0.8 ms after Pt nanoparticle adsorption (Supporting Information, Figure S3). The enhanced frequency response of CNT@m-C@Pt can be ascribed to the large and accessible surface area for ion accumulation and improved electron transport between the electrode and the current collector. According to previous studies on supercapacitor

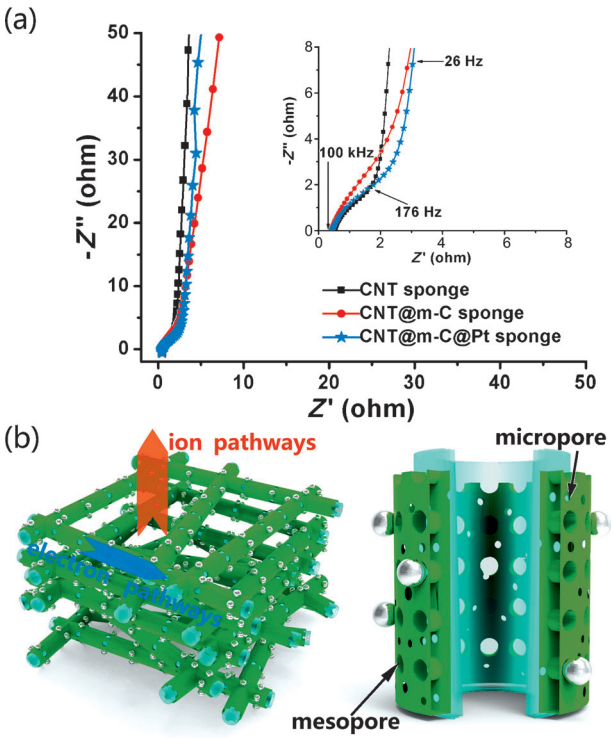

Figure 6. a) Electrochemical impedance spectroscopy of the CNT, CNT@m-C, and CNT@m-C@Pt sponges. Inset is the magnification of the high frequency region. b) Structural model of hierarchical CNT@m-C@Pt sponge.

electrodes incorporating Pt nanoparticles,[6] the enhanced specific capacitance was attributed to the effect of Pt on charge transfer rate from the electrolyte ions to the electrodes. The resistance across the electrolyte and interfacial resistance (R_e) for the CNT, CNT@m-C, and CNT@m-C@Pt sponge is 0.5, 0.44, and 0.3 Ω, respectively. The decreased resistance may be due to the efficient charge transfer from the electrode to the current collector, and these results are consistent with the electrical conductivity test results.

Figure 6b shows the structure model of hierarchical macro/meso sponge electrode in which the conductive CNT network acts as a support for m-C and Pt nanoparticles deposition, and the interconnected macropores between CNTs ensures efficient electrolyte ion diffusion and fast mass-transport through the electrode material. The energy storage occurs predominately in mesopores and the accessible micropores (interconnected graphitized layer spacing in m-C walls). In conclusion, the synergistic effect between each component enables an effective energy-storage system.

We also assembled a two-electrode configuration by placing two CNT@m-C or CNT@m-C@Pt sponges face to face separated by a filter paper. We can see in Figure 7a, the device based on two CNT@m-C@Pt sponge electrodes exhibits a nearly rectangular CV shape over a wide range of scan rates, suggesting an excellent capacitance behavior. The disappeared humps in CV curves are attributed to the symmetric electrode of supercapacitor devices. The CV and GC curves show a specific capacitance of 143 F g^{-1} for the CNT@m-C sponge, and 207 F g^{-1} for the CNT@m-C@Pt sponge (Figure 7b,c), which is significantly

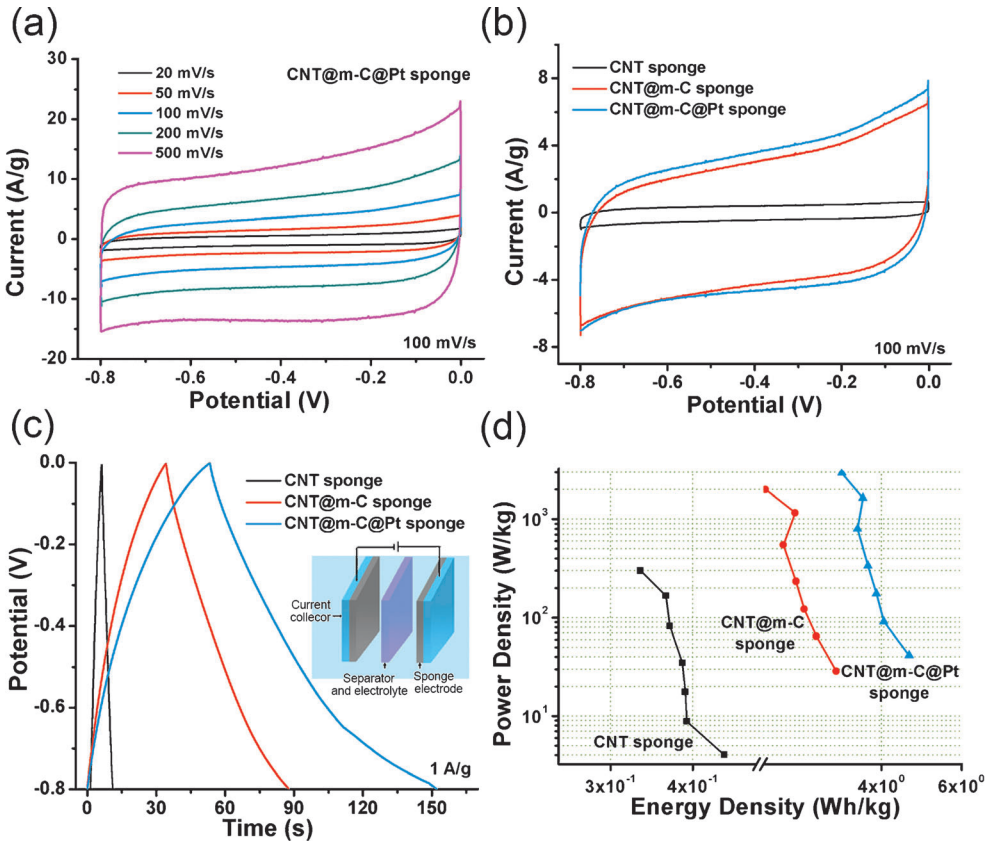

Figure 7. Design and fabrication of a two-electrode supercapacitor cell. a) CV curves of CNT@m-C@Pt supercapacitor at scan rates of 20, 50, 100, 200, 500 mV s^{-1}. b) CV curves of a symmetric two-electrode supercapacitor cell based on CNT, CNT@m-C, and CNT@m-C@Pt sponges collected at a scan rate of 100 mV s^{-1}. The rectangular CV shapes are observed for both sponge electrodes, indicating an efficient double-layer formation. c) GC curves of the corresponding cells recorded at 1 A g^{-1}. Inset, a symmetric two-electrode supercapacitor cell is constructed from two identical electrodes (the CNT@m-C or CNT@m-C@Pt sponge). d) Energy and power densities of CNT, CNT@m-C, and CNT@m-C@Pt supercapacitor cells. The CNT@m-C@Pt supercapacitor cell exhibits electrochemical energy storage with both high power and energy densities.

higher than that of the pure CNT sponge. The Ragone plot of the symmetric supercapacitor in Figure 7d illustrates the energy density versus power density performance, and we can see that supercapacitors based on CNT@m-C and CNT@m-C@Pt show increased power and energy density relative to the pure CNT sponge. The CNT@m-C@Pt supercapacitor exhibits an energy density of up to 4.6 W h kg^{-1} and retains 3.3 W h kg^{-1} at a high power density of 3000 W kg^{-1}. Furthermore, the three different supercapacitors all preserve more than 70% of their energy density as the power density increases.

We have adjusted the thickness of the m-C layer and loading of Pt nanoparticles to optimize the microstructure and supercapacitor performance. An optimal m-C coating thickness is found to be about 5 nm, whereas a thicker or thinner m-C coating results in decrease of specific capacitance (Supporting Information, Figure S4). Furthermore, adsorption of about 20 wt% Pt nanoparticles in the sponge leads to the maximum supercapacitor performance (Supporting Information, Figure S5).

Traditional m-C monolith is fragile and easily collapses under modest compression or deformation. Here, the CNT@m-C sponges are flexible and compressible owing to the presence of a stable and robust CNT 3D-network skeleton. A bulk CNT@m-C sponge is shown in Figure 8a, which can sustain large deformation without any structure damage, demonstrating good mechanical flexibility. Compressive stress–strain (σ–ε) curves show that the sponge can sustain uniaxial compression to large strains (up to 60%) and recover to original shape elastically (without residual strain) upon unloading (Figure 8b). The m-C coating also makes the CNTs thicker and reinforces the CNT sponge, and increases the compressive stress from 16 to 20 kPa at $\varepsilon = 50\%$ (Supporting Information, Figure S6a). Repeated large strain compression for 1000 cycles does not degrade the strength of the CNT@m-C sponge (Supporting Information, Figure S6).

Considering the mechanical flexibility of the CNT sponges, we tested their electrochemical performance under a compressed state. The CNT@m-C@Pt sponge exhibits similar CV curves at compressive strains of $\varepsilon = 20$ and 50%, with a capacitance retention of 99 and 96%, respectively, compared with the original state (Figure 8c). This indicates that under large degree compression, the 3D conductive CNT network can maintain an interconnected macro/meso structure and ensure high rate exchange and transport of ions and electrons, thus minimizing capacitance loss. Also, the GC curves of this sponge are almost identical in the original and compressed states, showing that the sponge can work stably even under very high compressive strains (up to 50%; Figure 8d). The EIS curves of the CNT@m-C@Pt sponge display a pure capacitive behavior without appreciable change in interfacial resistance in both states (Figure 8e). Even under the compressed state, the specific capacitance of our sponge electrodes could be retained well. When the scan rate increases from 2 to 200 mV s^{-1}, both CNT@m-C and CNT@m-C@Pt sponges show capacitance retention of about 70 and 80%, respectively, under compressive strains up to 50% (Supporting Information, Figure S7). This result indicates excellent rate performance and capacitance retention of our compressible sponge electrodes. These results indicate that our hybrid CNT sponges can serve as flexible supercapacitor electrodes and work under large degree compression without an appreciable capacitance drop. Furthermore, we also tested the supercapacitor cell performance under repeated

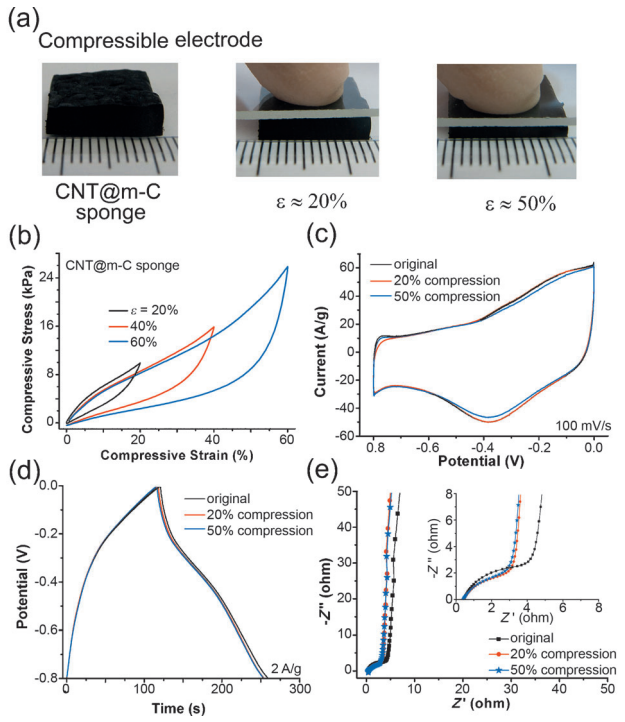

Figure 8. Supercapacitor performance of CNT@m-C@Pt sponge at a compressed state. a) Photos of a block of CNT@m-C sponge under manual compression at $\varepsilon = 20$, 50%. b) Compressive stress–strain curves of a CNT@m-C ($11.38 \times 9.60 \times 3.88$ mm^3) sponge at different strains of 20, 40, 60%, respectively. c) CV, d) GC, and e) EIS curves of CNT@m-C@Pt core–shell hybrid sponge at original, 20, and 50% compression state.

cyclic compression state. According to Figure S8 (Supporting Information), we can see that CNT@m-C and CNT@m-C@Pt sponge capacitor cells retain stable performance with a slight change under repeated cyclic compression tests.

During cyclic charging–discharging tests, the CNT@m-C and CNT@m-C@Pt sponges show an increase of specific capacitance to 284 and 498 F g^{-1} at 2 mV s^{-1}, respectively, within the first 200 cycles, and then stabilize until 1000 cycles (Supporting Information, Figure S9). After that, the specific capacitances have a decreased tendency but remain higher than the original after 5000 cycles. The capacitance enhancement during the first 200 cycles is attributed to two factors, namely 1) gradual electrolyte penetration into the graphitized m-C mesopores (pore walls in m-C walls) during the charging–discharging process, for it has been demonstrated that a suitable interlayer spacing can enhance the accumulation ability of electrolyte ions;[17] and 2) etching of m-C by potassium hydroxide and grafting of oxygen-containing functional groups on the electrode surface. Furthermore, the introduced defects on electrode surface allows wetting of previous inaccessible pores and increases contact surface for efficient electric double-layer formation.[16,18]

Conclusion

We have demonstrated a rational strategy to fabricate CNT@m-C@Pt sponges with controlled core–shell hybrid structures. The synergistic effect from the 3D conductive CNT network, the high surface area m-C coating, and the Pt nanoparticles as ion diffusion channels leads to significantly enhanced specific capacitance. The dense contact between CNTs and graphitic m-C were obtained by the CVD method, which ensures efficient electron transport and reduces electrical resistance between the two components. In contrast to traditional m-C, our sponges can be compressed to large strains and recover elastically, and work stably without appreciable capacitance degradation. Our hierarchical, macro/meso porous CNT-based hybrid sponges have potential applications as robust and flexible supercapacitor electrodes.

Acknowledgements

This work was supported by the National Nature Science Foundation of China (91127004, 51325202, 21201133, and 51272186) and Fundamental Research Funds for the Central Universities. Q.Y. thanks the large-scale instrument and equipment sharing foundation of Wuhan University.

Keywords: carbon · nanoparticles · nanotubes · mesoporous materials · platinum

[1] a) J. Chmiola, G. Yushin, Y. Gogotsi, C. Portet, P. Simon, P. L. Taberna, *Science* **2006**, *313*, 1760–1763; b) A. Kajdos, A. Kvit, F. Jones, J. Jagiello, G. Yushin, *J. Am. Chem. Soc.* **2010**, *132*, 3252–3253.

[2] a) P. Simon, Y. Gogotsi, *Nature Mater.* **2008**, *7*, 845–854; b) M. Endo, Y. J. Kim, H. Ohta, K. Ishii, *Carbon* **2002**, *40*, 2613–2626; c) L. Z. Fan, Y. H. Hu, J. Maier, P. Adelhelm, B. Smarsly, M. Antonietti, *Adv. Funct. Mater.* **2007**, *17*, 3083–3087; d) T. C. Weng, H. Teng, *J. Electrochem. Soc.* **2001**, *148*, A368–A373; e) C. Largeot, C. Portet, J. Chmiola, P. L. Taberna, Y. Gogotsi, P. Simon, *J. Am. Chem. Soc.* **2008**, *130*, 2730–2731; f) C. O. Ania, V. Khomenko, E. R. Piñero, J. B. Parra, F. Béguin, *Adv. Funct. Mater.* **2007**, *17*, 1828–1836.

[3] a) W. R. Li, D. H. Chen, Z. Li, Y. F. Shi, D. Y. Zhao, Z. Y. Jiang, *Electrochem. Commun.* **2007**, *9*, 569–573; b) C. Guan, Z. Y. Zeng, X. L. Li, H. Zhang, H. J. Fan, *Small* **2014**, *10*, 300–307; c) H. Nishihara, T. Kyotani, *Adv. Mater.* **2012**, *24*, 4473–4498; d) Y. P. Zhai, Y. Q. Dou, D. Y. Zhao, P. F. Fulvio, R. T. Mayes, S. Dai, *Adv. Mater.* **2011**, *23*, 4828–4850; e) K. X. Wang, Y. G. Wang, Y. R. Wang, E. Hosono, H. S. Zhou, *J. Phys. Chem. C* **2009**, *113*, 1093–1097; f) J. Wei, D. D. Zhou, Z. K. Sun, Y. H. Deng, Y. Y. Xia, D. Y. Zhao, *Adv. Funct. Mater.* **2013**, *23*, 2322–2328; g) Y. G. Wang, H. Q. Li, Y. Y. Xia, *Adv. Mater.* **2006**, *18*, 2619–2623; h) M. C. Orilall, U. Wiesner, *Chem. Soc. Rev.* **2011**, *40*, 520–535; i) X. H. Xia, D. L. Chao, Z. X. Fan, H. Zhang, H. J. Fan, *Nano Lett.* **2014**, *14*, 1651–1658; j) A. Vu, Y. Q. Qian, A. Stein, *Adv. Energy Mater.* **2012**, *2*, 1056–1085; k) H. C. Bi, X. Huang, X. Wu, L. T. Sun, H. Zhang, *Small* **2014**, DOI: 10.1002/smll.201303413; l) Y. Fang, Y. Y. Lv, R. C. Che, H. Y. Wu, D. Y. Zhao, *J. Am. Chem. Soc.* **2013**, *135*, 1524–1530.

[4] X. F. Qian, Y. Y. Lv, W. Li, Y. Y. Xia, D. Y. Zhao, *J. Mater. Chem.* **2011**, *21*, 13025–13031.

[5] T. Tao, L. Zhang, H. Jiang, C. Z. Li, *New J. Chem.* **2013**, *37*, 1294–1297.

[6] a) E. Taer, M. Deramana, I. A. Taliba, S. A. Hashmic, A. A. Umar, *Electrochim. Acta* **2011**, *56*, 10217–10222; b) Q. L. Zhang, Y. W. Zhang, Z. H. Gao, H. L. Ma, J. Q. Li, M. L. Zhai, *J. Mater. Chem. C* **2013**, *1*, 321–328.

[7] X. C. Gui, J. Q. Wei, K. L. Wang, A. Y. Cao, H. W. Zhu, D. H. Wu, *Adv. Mater.* **2010**, *22*, 617–621.

[8] Y. B. Yang, E. Z. Shi, P. X. Li, D. H. Wu, S. T. Wu, A. Y. Cao, Q. Yuan, *Nanoscale* **2014**, *6*, 3585–3592.

[9] W. J. Gao, Y. Wan, Y. Q. Dou, D. Y. Zhao, *Adv. Energy Mater.* **2011**, *1*, 115–123.

[10] A. H. Lu, W. C. Li, G. P. Hao, B. Spliethoff, F. Schüth, *Angew. Chem. Int. Ed.* **2010**, *49*, 1615–1618; *Angew. Chem.* **2010**, *122*, 1659–1662.

[11] N. P. Wickramaratne, V. S. Perera, B. W. Park, M. Jaroniec, *Chem. Mater.* **2013**, *25*, 2803 – 2811.
[12] S. B. Yoon, G. S. Chai, S. K. Kang, J. S. Yu, K. P. Gierszal, M. Jaroniec, *J. Am. Chem. Soc.* **2005**, *127*, 4188 – 4189.
[13] D. Y. Qu, H. Shi, *J. Power Sources* **1998**, *74*, 99 – 107.
[14] Y. R. Liang, D. C. Wu, R. W. Fu, *Langmuir* **2009**, *25*, 7783 – 7785.
[15] M. C. Gutiérrez, F. Picó, F. Rubio, F. D. Monte, J. M. Rojo, *J. Mater. Chem.* **2009**, *19*, 1236 – 1240.
[16] M. Rose, Y. Korenblit, E. Kockrick, G. Yushin, *Small* **2011**, *7*, 1108 – 1117.
[17] J. J. Yoo, K. Balakrishnan, J. S. Huang, V. Meunier, P. M. Ajayan, *Nano Lett.* **2011**, *11*, 1423 – 1427.
[18] A. G. Pandolfo, A. F. Hollenkamp, *J. Power Sources* **2006**, *157*, 11 – 27.

Received: November 24, 2014
Revised: December 16, 2014
Published online on ■■ ■■, 2015

FULL PAPER

Hybrid sponge: A rational strategy was developed by using a carbon nanotube (CNT) sponge as a 3D network template to fabricate hierarchical porous CNT@m-C@Pt core–shell hybrid structures (see picture: blue CNTs, green m-C (mesoporous carbon), silver Pt nanoparticles). These hybrid sponges show promising applications as high-performance flexible supercapacitor electrodes.

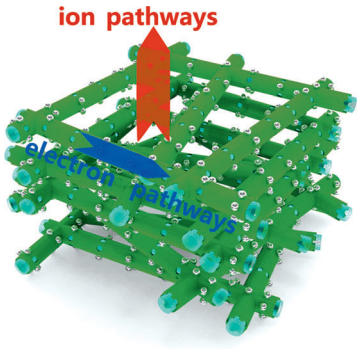

Mesoporous Materials

Y. Yang, P. Li, S. Wu, X. Li, E. Shi, Q. Shen, D. Wu, W. Xu, A. Cao, Q. Yuan**

■■ – ■■

Hierarchically Designed Three-Dimensional Macro/Mesoporous Carbon Frameworks for Advanced Electrochemical Capacitance Storage